

Development of long-range phase coherence on the Kondo lattice

Jian-Jun Dong^{1,2,3} and Yi-feng Yang^{2,3,4,*}

¹*Department of Physics and Chongqing Key Laboratory for Strongly Coupled Physics, Chongqing University, Chongqing 401331, China*

²*Beijing National Laboratory for Condensed Matter Physics and Institute of Physics, Chinese Academy of Sciences, Beijing 100190, China*

³*University of Chinese Academy of Sciences, Beijing 100049, China*

⁴*Songshan Lake Materials Laboratory, Dongguan, Guangdong 523808, China*

(Dated: October 28, 2022)

Despite of many efforts, we still lack a clear picture on how heavy electrons emerge and develop on the Kondo lattice. Here we introduce a key concept named the hybridization bond phase and propose a scenario based on phase correlation to address this issue. The bond phase is a gauge-invariant quantity combining two onsite hybridization fields mediated by inter-site magnetic correlations. Its probabilistic distribution decays exponentially with site distance, from which a characteristic length scale can be extracted to describe the spatial correlation of Kondo hybridizations. Our calculations show that this correlation length grows logarithmically with lowering temperature at large Kondo coupling, and reveal a precursor pseudogap state with short-range phase correlation before long-range phase coherence is developed to form the Kondo insulating (or heavy electron) state at low temperatures. This provides a potential microscopic explanation of the two-stage hybridization proposed by recent pump-probe experiment and the logarithmic scaling in the phenomenological two-fluid model. Our work offers a novel theoretical framework to describe the phase-related physics in Kondo lattice systems.

Heavy fermion systems are featured with correlated phenomena such as unconventional superconductivity, quantum criticality, and non-Fermi liquid [1–4]. Underlying all these exotic properties is the interplay of inter-site magnetic correlations and spin screening as described by the Kondo lattice model [5–7]. It differs from the single-impurity Kondo physics in that the many-body spin-entangled state between local moments and conduction electrons can extend and propagate on the lattice as dispersive heavy electrons. But how this state emerges, develops and eventually extends in space remains less understood despite many theoretical efforts [8]. In particular, recent angle-resolved photoemission spectroscopy (ARPES) experiment reported the onset of hybridization well above the coherence temperature in transport measurements [9, 10]. Later pump probe experiment revealed a two-stage process for the heavy electron development on the lattice [11, 12]. This two-stage scenario seems quite universal [13], but still awaits a microscopic explanation. Its theoretical formulation will necessarily deepen our understanding of the Kondo lattice physics.

Phase fluctuations play an indispensable role in modern strongly correlated physics and have been extensively studied in past decades. Notable examples include deconfined phases in lattice gauge theories [14–16], phase-fluctuation scenario in high- T_c cuprates [17–20], and flux phases in quantum spin liquids [21–23]. In Kondo lattice systems, phase fluctuations appear when some slave particles or auxiliary fields are introduced to describe local spins and their entanglement with conduction electrons, but were often ignored in prevailing mean-field calculations, causing artificial finite-temperature phase transitions [24–29]. Phase fluctuations can convert these arti-

ficial transitions into a crossover [30, 31], and may be a key controlling the development of heavy electron state beyond usual mean-field or local approximations [32–41], but a proper description is not yet available.

In this work, we address this issue by proposing a novel theoretical framework to describe heavy electron emergence based on phase coherence. We employ a recently-proposed static auxiliary field approach for Kondo systems [42] and introduce a gauge-invariant bond phase to characterize spatial correlation of the hybridization fields. This bond phase combines the onsite hybridization fields and inter-site magnetic correlation fields between two spatially separated lattice sites, so its probabilistic distribution tracks directly the spatial development of heavy electron state. Our calculations show a logarithmic temperature dependence of its characteristic length scale and reveal a precursor short-range phase-correlated pseudogap state before the long-range phase coherence is developed to form the Kondo insulating or heavy electron state at lower temperatures. Our theory provides a general scheme to describe the phase coherence and other phase-related physics in Kondo lattice systems.

For simplicity, we consider the two-dimensional Kondo-Heisenberg model on a square lattice,

$$H = -t \sum_{\langle ij \rangle \sigma} \left(c_{i\sigma}^\dagger c_{j\sigma} + \text{H.c.} \right) + J_K \sum_i \mathbf{s}_i \cdot \mathbf{S}_i + J_H \sum_{\langle ij \rangle} \mathbf{S}_i \cdot \mathbf{S}_j, \quad (1)$$

where t is the hopping integral of conduction electrons between nearest-neighbor sites, $\mathbf{s}_i = \sum_{\alpha\beta} c_{i\alpha}^\dagger \frac{\boldsymbol{\sigma}_{\alpha\beta}}{2} c_{i\beta}$ is the conduction electron spin localized at \mathbf{r}_i , and \mathbf{S}_i denotes the local spins. J_K and J_H describe the Kondo and Heisenberg exchange interactions. Under the Abrikosov

pseudofermion representation $\mathbf{S}_i = \sum_{\eta\gamma} f_{i\eta}^\dagger \frac{\sigma_{\eta\gamma}}{2} f_{i\gamma}$, both terms can be decoupled using the Hubbard-Stratonovich transformation: $2\mathbf{s}_i \cdot \mathbf{S}_i \rightarrow \sum_{\sigma} (V_i c_{i\sigma}^\dagger f_{i\sigma} + \text{H.c.}) + |V_i|^2$ and $2\mathbf{S}_i \cdot \mathbf{S}_j \rightarrow \sum_{\sigma} (\chi_{ij} f_{i\sigma}^\dagger f_{j\sigma} + \text{H.c.}) + |\chi_{ij}|^2$, where V_i and χ_{ij} are two fluctuating auxiliary fields describing the hybridization and inter-site magnetic correlation, respectively. This gives the action [43]:

$$S = \sum_{i,l} \frac{\beta J_K |V_{i,l}|^2}{2} + \sum_{(ij),l} \frac{\beta J_H |\chi_{ij,l}|^2}{2} - \sum_i \beta \lambda_i + \sum_{nm\sigma} \Psi_{n\sigma}^\dagger (O_{nm} - i\omega_n \delta_{nm}) \Psi_{m\sigma}, \quad (2)$$

where $\Psi_{n\sigma} = [c_{1\sigma n}, \dots, c_{N_0\sigma n}, f_{1\sigma n}, \dots, f_{N_0\sigma n}]^T$, N_0 is the number of lattice sites, and the subscripts l (n/m) denote bosonic (fermionic) Matsubara frequency. λ_i is the Lagrange multiplier for the constraint $\sum_{\sigma} f_{i\sigma}^\dagger f_{i\sigma} = 1$ and takes a real value after Wick rotation [22].

The above action is generally impossible to solve. To proceed, we adopt a static approximation, $V_{i,n-m} = V_i \delta_{nm}$, $\chi_{ij,n-m} = \chi_{ij} \delta_{nm}$ such that $O_{nm} = O \delta_{nm}$. This ignores temporal fluctuations of the auxiliary fields but takes full account of their spatial fluctuations and statistical distribution [44–47]. The fermions can be integrated out, giving an effective action only of the auxiliary fields:

$$S_{\text{eff}} = \sum_i \frac{\beta J_K |V_i|^2}{2} + \sum_{(ij)} \frac{\beta J_H |\chi_{ij}|^2}{2} - \sum_i \beta \lambda_i - 2 \sum_n \ln \det (O - i\omega_n). \quad (3)$$

The matrix O has a block form $O = \begin{bmatrix} T^c & M \\ M^\dagger & T^f \end{bmatrix}$, where T^c (T^f) is the $N_0 \times N_0$ hopping matrix of conduction electrons (pseudofermions), and $M_{ij} = \delta_{ij} J_K V_i / 2$ is a diagonal matrix for their onsite hybridization. The summation over Matsubara frequency can be evaluated using $\sum_n \ln \det (O - i\omega_n) = \sum_l \ln (1 + e^{-\beta \xi_l})$, where ξ_l is the eigenvalues of O and always real because O is Hermitian. The probabilistic distribution of the auxiliary fields is then simply, $p(V_i, \chi_{ij}) = Z^{-1} e^{-S_{\text{eff}}}$, where Z is the partition function serving as the normalization factor. It can be simulated using the Monte Carlo and Metropolis algorithm on $3N_0$ complex random variables without sign problem [48–50]. This is different from the (non-uniform) mean-field method where the auxiliary variables take fixed values determined by the saddle-point approximation. For simplicity, we set the half conduction bandwidth to unity ($t = 1/4$), fix $J_H = 0.2$, and consider only the particle-hole symmetric model on a $N_0 = 8 \times 8$ lattice where the Lagrangian multipliers are approximated by their saddle-point value $\lambda_i = 0$ [51]. Other choices of parameters or a larger lattice have been examined and the conclusions are qualitatively unchanged.

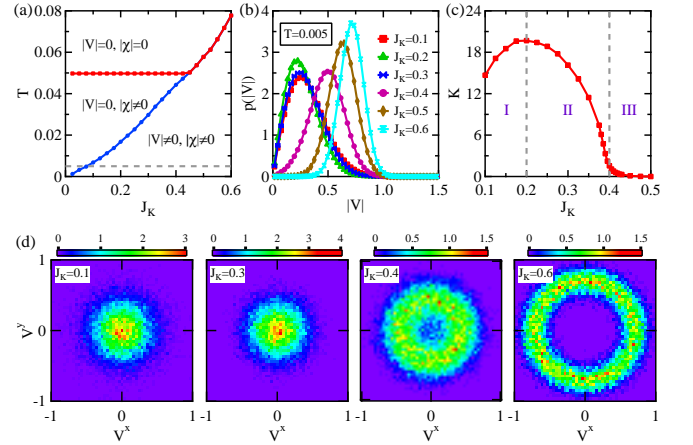


FIG. 1: (a) The mean-field phase diagram predicted under uniform approximation. The dashed line marks the temperature $T = 0.005$. (b) The amplitude probabilistic distribution $p(|V|)$ for different J_K at $T = 0.005$. (c) The slope $K = dp(|V|)/d|V|$ at $|V| = 0$ showing three different regions. (d) Density plots of $p(V)$ on complex plane $V = (V^x, V^y)$ for four chosen values of J_K at $T = 0.005$.

For comparison, we first show the usual mean-field phase diagram in Fig. 1(a), where the auxiliary fields are assumed to be uniform and real: $V_i = \bar{V}_i = V$, $\chi_{ij} = \bar{\chi}_{ij} = \chi$. The solution can be obtained by minimizing the free energy $F = S_{\text{eff}}/\beta$ [43]. With lowering temperature, we see a second-order phase transition from $\chi = 0$ to $\chi \neq 0$ at $T = J_H/4$, below which there is a weakly coupled state of conduction electrons and spin liquid [30]. Increasing J_K drives the system into a Kondo insulating state with nonzero V .

We may examine this mean-field picture by considering the probabilistic distribution of the complex hybridization fields, $p(V) \equiv p(V_i)$, which is the same on all sites due to translational symmetry and can be evaluated using the Metropolis algorithm for importance sampling of the effective action Eq. (3) [43]. Figure 1(b) plots the marginal distribution of its amplitude, $p(|V|)$, at a low temperature after integrating out all other variables. The maximum of $p(|V|)$ is seen to vary nonmonotonically with increasing J_K . As shown in Fig. 1(c), we may identify three regions according to the slope $K = dp(|V|)/d|V|$ at $|V| = 0$. Figure 1(d) plots the distribution $p(V)$ on the complex plane $V = (V^x, V^y)$. As expected, the data cluster around $(0,0)$ at small J_K and turn into a ring at large J_K . The distribution is therefore dominated by the bare fluctuation term $\beta J_K |V|^2/2$ in region I and the coupling with conduction electrons in region III, while region II marks a crossover in between.

The difference from the mean-field solution can be revealed by studying phase fluctuations of the auxiliary fields. Since the effective action (3) is invariant under the gauge transformation $V_i \rightarrow V_i e^{i\beta_i}$, $\chi_{ij} \rightarrow e^{-i(\beta_i - \beta_j)}$,

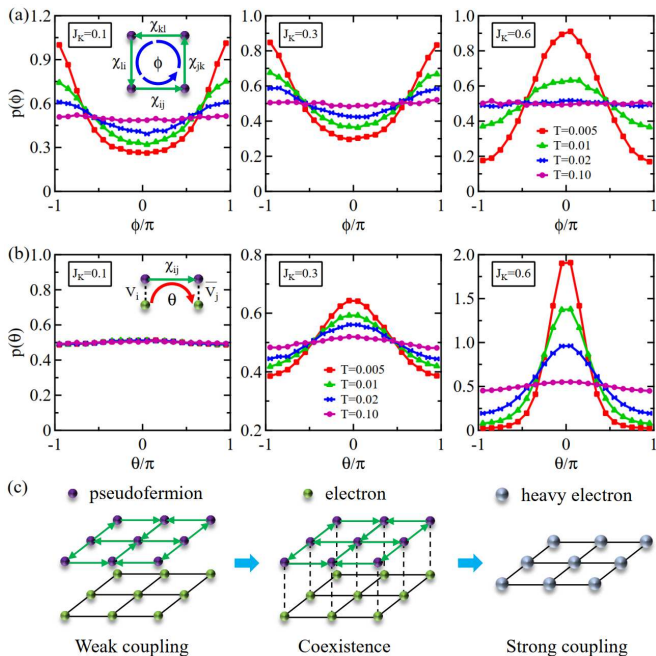


FIG. 2: Comparison of the probabilistic distribution of (a) the flux $p(\phi)$ and (b) the bond phase $p(\theta)$ for three typical values of J_K . The insets illustrate the definition of flux and bond phases. (c) Schematic plots of the coupling between pseudofermions and conduction electrons in three different low-temperature regions.

we may define two gauge-invariant phases from

$$\begin{aligned} F_i &\equiv \chi_{ij}\chi_{jk}\chi_{kl}\chi_{li} = |F_i| e^{i\phi_i}, \\ B_{ij} &\equiv V_i\chi_{ij}\bar{V}_j = |B_{ij}| e^{i\theta_{ij}}, \end{aligned} \quad (4)$$

where ϕ_i denotes the flux in a plaquette $ijkl \in \square$ and θ_{ij} reflects the phase of the hybridization bond B_{ij} between nearest-neighbor sites ij as illustrated in the insets of Fig. 2. The bond phase θ_{ij} reflects the correlation of two onsite hybridization fields V_i and V_j mediated by their inter-site magnetic correlation χ_{ij} . It by definition contains spatial correlation information and is a key quantity introduced in this work to distinguish the Kondo lattice physics from the single-impurity Kondo physics [52–55].

Figures 2(a) and 2(b) plot their probabilistic distributions for three typical values of J_K . Again, due to translational symmetry, we drop the site subscript and use $p(\phi) \equiv p(\phi_i)$ and $p(\theta) \equiv p(\theta_{ij})$. For weak coupling $J_K = 0.1$, the local spins and conduction electrons are almost decoupled. The bond phase $p(\theta)$ distributes uniformly at all temperatures, while the flux distribution $p(\phi)$ becomes peaked at $\phi = \pi$ below certain temperature. The latter indicates a π -flux state [56–59], which is a special feature of the pseudofermion representation of the Heisenberg model on the two-dimensional lattice and might be realized if the spin interaction is highly frustrated or on an optical lattice. Our results are in ac-

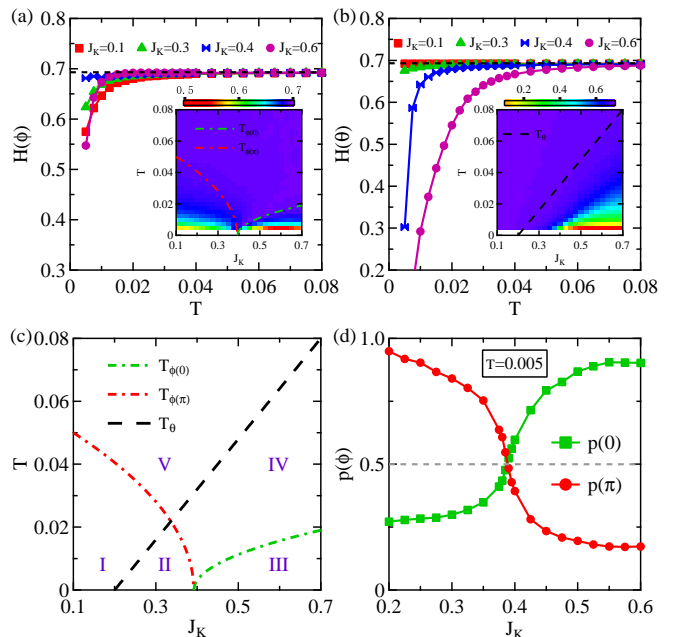


FIG. 3: The Shannon entropy of (a) the flux ϕ/π and (b) the bond phase θ/π as functions of temperature for different values of J_K . The black dashed line marks the uniform limit $\ln 2$. The insets are the intensity plot of the Shannon entropy on the T - J_K plane, showing different behaviors of flux and bond phases at low temperatures. The lines are a guide to the eye separating the diagram into different tentative regions. (c) A schematic T - J_K phase diagram constructed based on the intensity plots, where T_θ marks a crossover between uniform and non-uniform distribution of the bond phase, and $T_{\phi(0)}$ ($T_{\phi(\pi)}$) marks a crossover to the non-uniform flux distribution peaked at $\phi = 0$ (π). (d) Comparison of the flux probabilistic distribution $p(\phi)$ at $\phi = 0$ and π as a function of the Kondo coupling at a very low temperature $T = 0.005$.

cordance with Lieb’s theorem [60], which states that the saddle point for a half-filled band of fermions hopping on a planar lattice is π per plaquette. This implies that our approach can capture the correct saddle point beyond the ad hoc uniform mean-field approximation. The π -flux state may not be stable in general situations, giving rise to confined states like antiferromagnetic order or magnon excitations. For simplicity, we ignore all these complications and take it as our starting point in order to focus on the Kondo aspect of the model. For an intermediate $J_K = 0.3$, we still have π -flux, but the bond phase distribution becomes non-uniform at low temperatures with a peak around $\theta = 0$, indicating the onset of phase correlation between nearest-neighbor hybridization fields. It therefore marks a coexisting state of flux and hybridization correlation. For strong coupling $J_K = 0.6$, the location of maximal $p(\phi)$ changes from $\phi = \pi$ to $\phi = 0$, indicating that the π -flux is completely suppressed and the system enters the Kondo insulating (or heavy electron) state. Figure 2(c) gives an illustration of all three low-

temperature states. For completeness, the probabilistic distributions of $|F_i|$ and $|B_{ij}|$ are also given in the Supplemental Material [43].

The variation of the probabilistic distributions may be reflected also in their Shannon entropy defined as $H(x) \equiv -\int p(x) \ln p(x) dx$ for a continuous random variable x with the probabilistic distribution $p(x)$. The results are plotted in Figs. 3(a) and 3(b). As expected, the Shannon entropies for both ϕ/π and θ/π approach their uniform limit $\ln 2$ at high temperatures. Deviation from $\ln 2$ defines a crossover temperature scale for the onset of non-uniform probabilistic distribution due to either flux or bond phase correlation. A tentative phase diagram can then be constructed based on the intensity plots in the insets and the amplitude analysis in Fig. 1(c). As shown in Fig. 3(c), the dashed line T_θ marks a crossover to the region with non-uniform $p(\theta)$, while the dash-dotted lines, $T_{\phi(\pi)}$ and $T_{\phi(0)}$, mark the crossover to π or 0-flux dominated regions, respectively. Note that these lines are not phase transitions but only serve as a tentative guide to the eye. Approaching zero temperature, as shown in Fig. 3(d), the curves of $p(\phi)$ at $\phi = \pi$ and $\phi = 0$ as a function of J_K cross each other exactly at the transition between regions II and III, indicating that the flux phase ϕ distributes uniformly and restores its full symmetry at this point. The phase diagram is therefore divided tentatively into five regions: region I is dominated by π -flux; region II is a crossover with coexisting π -flux and hybridization (bond phase) correlation; regions III and IV are dominated mostly by hybridization; region V contains weakly coupled local spins and almost decoupled conduction electrons. To exclude possible finite size effect, we have performed calculations on a 24×24 lattice using the traveling cluster approximation method [61], and the results confirmed all five regions.

To clarify the hybridization properties in regions II-IV, we extend the definition of the bond phase to

$$\begin{aligned} \theta_R &\equiv \theta_{i_0 i_1} + \theta_{i_1 i_2} + \cdots + \theta_{i_{R-1} i_R} \bmod 2\pi \\ &= \text{Im} \ln (V_{i_0} \chi_{i_0 i_1} \bar{V}_{i_1} V_{i_1} \chi_{i_1 i_2} \cdots \chi_{i_{R-1} i_R} \bar{V}_{i_R}), \end{aligned} \quad (5)$$

where $i_0 i_1 i_2 \dots i_R$ denotes a path of length R linking two end sites at \mathbf{r}_{i_0} and $\mathbf{r}_{i_R} \equiv \mathbf{r}_{i_0} + \mathbf{R}$. Since $\bar{V}_j V_j = |V_j|^2$ do not contribute a phase, we have also $\theta_R = \text{Im} \log(V_{i_0} \chi_{i_0 i_1} \chi_{i_1 i_2} \cdots \chi_{i_{R-1} i_R} \bar{V}_{i_R})$, which is a gauge-invariant quantity describing phase correlation of the hybridization fields on two end sites mediated by inter-site magnetic correlations along the path. Figures 4(a)-4(c) compare the distribution $p(\theta_R)$ for different R in regions II, III, and IV, respectively. We find it rapidly decays to uniform distribution with increasing R in II and IV but remains peaked at $\theta_R = 0$ in region III.

To quantify this decay, we plot in Fig. 4(d) the probability $p(\theta_R = 0)$ at $J_K = 0.6$ as a function of the length R for the shortest path linking two sites and fit the curves with an exponential function $p(\theta_R = 0) = A e^{-R/\xi} + B$

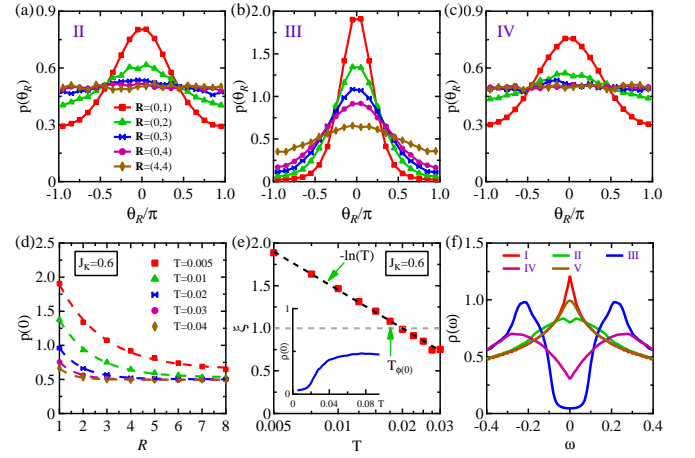


FIG. 4: The probabilistic distribution $p(\theta_R)$ for a shortest path between two end sites with $\mathbf{R} = (R_x, R_y)$ in regions (a) II, (b) III, and (c) IV. The distribution is always uniform in regions I and V and therefore not shown. (d) The probability $p(\theta_R = 0)$ as a function of the path length R ($\equiv |R_x| + |R_y|$) for different temperatures at $J_K = 0.6$. The dashed line is the fit using $A e^{-R/\xi} + B$. (e) The extracted correlation length ξ as a function of temperature at $J_K = 0.6$. We find ξ follows a logarithmic temperature dependence (dashed line) and is roughly one near $T_{\phi(0)}$. The conduction electron density of states at $\omega = 0$ (inset) shows that the Kondo insulating (or indirect hybridization) gap opens roughly below the same temperature, with a precursor pseudogap state at higher temperatures. (f) Comparison of typical conduction electron density of states in different regions of the phase diagram. The parameters are chosen as $T = 0.005$, $J_K = 0.1$ for region I; $T = 0.005$, $J_K = 0.35$ for II; $T = 0.005$, $J_K = 0.6$ for III; $T = 0.03$, $J_K = 0.6$ for IV; $T = 0.08$, $J_K = 0.1$ for V.

(dashed lines). This allows us to extract a characteristic correlation length ξ which reflects an effective spatial extension of the influence of the hybridization at one site to reach other sites on the Kondo lattice. As shown in Fig. 4(e), ξ is less than 1 (in the unit of lattice parameter) at high temperatures but increases logarithmically (dashed line) with lowering temperature. The latter seems to be consistent with the phenomenological two-fluid model [62–64]. Remarkably, the temperature where $\xi \approx 1$ agrees roughly with $T_{\phi(0)}$, the crossover between regions III and IV estimated from the Shannon entropy. Thus, region IV (and II) represents a state where the phase correlation is developed only on short range between nearest-neighbor sites, while in region III, the hybridization fields start to extend their influence in space and build a long-range phase coherence on the lattice.

A direct consequence of the phase correlation may be found on the conduction electron density of states $\rho(\omega)$ calculated using Eq. (2). A twisted boundary condition $c_j^\dagger \rightarrow c_j^\dagger e^{i\psi \cdot \mathbf{r}_j}$ was used to reduce the finite size effect and obtain a smooth curve [65, 66]. The results are presented in Fig. 4(f) after being averaged over 20×20 twisted

boundary configurations of $\psi = (\psi_x, \psi_y)$ with both ψ_x and ψ_y regularly spaced in $\left[0, \frac{2\pi}{\sqrt{N_0}}\right)$. We find that the conduction electron spectra are barely affected in regions I and V, while a pseudogap is developed in regions II and IV where the hybridization bond phase is short-range correlated. This is associated with the ARPES band bending due to the opening of direct hybridization gap [9]. Only in region III, we see a fully opened (indirect hybridization) gap with a small remaining spectral weight around $\omega \approx 0$ due to Lorentzian broadening ($\delta = 0.01$) used in the calculations. The full gap opening temperature is in rough accordance with the growth of ξ in the bond phase distribution, as compared in the inset of Fig. 4(e) for $J_K = 0.6$. Thus, the heavy electron emergence or Kondo insulating state is closely related to the development of long-range phase coherence of hybridization fields mediated by inter-site magnetic correlations, suggesting the importance of our defined bond phase in describing heavy fermion physics beyond the usual mean-field picture and local approximations. The distinction of short- and long-range phase correlations provides a potential microscopic explanation of the two-stage scenario for the pump-probe experiment [11, 13] and lays a theoretical basis for resolving the conflict between ARPES and transport data [9].

To summarize, we propose a novel scheme to study the hybridization physics of Kondo lattice systems based on static auxiliary field approximation. A gauge-invariant hybridization bond phase is introduced to investigate the spatial phase correlation of the hybridization fields. Its probabilistic distribution allows us to define a characteristic length scale which diverges logarithmically with lowering temperature. A precursor pseudogap state with short-range phase correlation is revealed, before the Kondo insulating (or heavy electron) state emerges when a long-range phase coherence starts to develop. This provides a possible microscopic support of the two-stage hybridization scenario suggested by recent experiment. Our work proposes a novel framework based on spatial phase correlation beyond conventional mean-field and local pictures, and offers a useful tool to explore phase-related physics in Kondo lattice systems.

We acknowledge useful discussions with Yin Zhong. This work was supported by the National Natural Science Foundation of China (NSFC Grants No. 12204075, No. 11974397, No. 12174429, and No. 12147102), the National Key Research and Development Program of MOST of China (Grant No. 2017YFA0303103), and the Strategic Priority Research Program of the Chinese Academy of Sciences (Grant No. XDB33010100).

* yifeng@iphy.ac.cn

[1] M. Sgrist and K. Ueda, Phenomenological theory of un-

conventional superconductivity, Rev. Mod. Phys. **63**, 239 (1991).

- [2] G. R. Stewart, Non-Fermi-liquid behavior in d - and f -electron metals, Rev. Mod. Phys. **73**, 797 (2001).
- [3] P. Gegenwart, Q. Si, and F. Steglich, Quantum criticality in heavy-fermion metals, Nat. Phys. **4**, 186 (2008).
- [4] Y.-F. Yang and D. Pines, Emergent states in heavy electron materials, Proc. Natl. Acad. Sci. USA **109**, E3060 (2012).
- [5] A. C. Hewson, *The Kondo Problem to Heavy Fermions*, (Cambridge University Press, Cambridge, England, 1997).
- [6] P. Coleman, *Introduction to Many-body Physics*, (Cambridge University Press, Cambridge, England, 2015).
- [7] Y.-F. Yang, D. Pines, and G. Lonzarich, Quantum critical scaling and fluctuations in Kondo lattice materials, Proc. Natl. Acad. Sci. USA **114**, 6250 (2017).
- [8] G. Lonzarich, D. Pines, and Y.-F. Yang, Toward a new microscopic framework for Kondo lattice materials, Rep. Prog. Phys. **80**, 024501 (2017).
- [9] Q. Y. Chen, D. F. Xu, X. H. Niu, J. Jiang, R. Peng, H. C. Xu, C. H. P. Wen, Z. F. Ding, K. Huang, L. Shu, Y. J. Zhang, H. Lee, V. N. Strocov, M. Shi, F. Bisti, T. Schmitt, Y. B. Huang, P. Dudin, X. C. Lai, S. Kirchner, H. Q. Yuan, and D. L. Feng, Direct observation of how the heavy-fermion state develops in CeCoIn₅, Phys. Rev. B **96**, 045107 (2017).
- [10] Y.-F. Yang, Two-fluid model for heavy electron physics, Rep. Prog. Phys. **79**, 074501 (2016).
- [11] Y. P. Liu, Y. J. Zheng, J.-J. Dong, H. Lee, Z. X. Wei, W. L. Zhang, C. Y. Chen, H. Q. Yuan, Y.-F. Yang, and J. Qi, Hybridization Dynamics in CeCoIn₅ Revealed by Ultrafast Optical Spectroscopy, Phys. Rev. Lett. **124**, 057404 (2020).
- [12] D. Hu, J.-J. Dong, and Y.-F. Yang, Hybridization fluctuations in the half-filled periodic Anderson model, Phys. Rev. B **100**, 195133 (2019).
- [13] Y. H. Pei, Y. J. Zhang, Z. X. Wei, Y. X. Chen, K. Hu, Yi-feng Yang, H. Q. Yuan, and J. Qi, Unveiling the hybridization process in a quantum critical ferromagnet by ultrafast optical spectroscopy, Phys. Rev. B **103**, L180409 (2021).
- [14] J. B. Kogut, An introduction to lattice gauge theory and spin systems, Rev. Mod. Phys. **51**, 659 (1979).
- [15] S. Gazit, M. Randeria, and A. Vishwanath, Emergent Dirac fermions and broken symmetries in confined and deconfined phases of Z_2 gauge theories, Nat. Phys. **13**, 484 (2017).
- [16] X. Y. Xu, Y. Qi, L. Zhang, F. F. Assaad, C. Xu, and Z. Y. Meng, Monte Carlo Study of Lattice Compact Quantum Electrodynamics with Fermionic Matter: The Parent State of Quantum Phases, Phys. Rev. X **9**, 021022 (2019).
- [17] M. Mayr, G. Alvarez, C. Sen, and E. Dagotto, Phase Fluctuations in Strongly Coupled d-Wave Superconductors, Phys. Rev. Lett. **94**, 217001 (2005).
- [18] G. Alvarez and E. Dagotto, Fermi Arcs in the Superconducting Clustered State for Underdoped Cuprate Superconductors, Phys. Rev. Lett. **101**, 177001 (2008).
- [19] Y. Dubi, Y. Meir, and Y. Avishai, Nature of the superconductor-insulator transition in disordered superconductors, Nature (London) **449**, 876 (2007).
- [20] Q. Han, T. Li, and Z. D. Wang, Pseudogap and Fermi-arc evolution in the phase-fluctuation scenario, Phys. Rev. B

- 82**, 052503 (2010).
- [21] X.-G. Wen, *Quantum Field Theory of Many-Body Systems: From the Origin of Sound to an Origin of Light and Electrons*, (Oxford University Press, New York, 2004).
- [22] Y. Zhou, K. Kanoda, and T.-K. Ng, Quantum spin liquid states, *Rev. Mod. Phys.* **89**, 025003 (2017).
- [23] R. Wang, Y. Wang, Y. X. Zhao, and B. Wang, Emergent Kondo Behavior from Gauge Fluctuations in Spin Liquids, *Phys. Rev. Lett.* **127**, 237202 (2021).
- [24] A. Auerbach and K. Levin, Kondo Bosons and the Kondo Lattice: Microscopic Basis for the Heavy Fermi Liquid, *Phys. Rev. Lett.* **57**, 877 (1986).
- [25] D. M. Newns and N. Read, Mean-field theory of intermediate valence/heavy fermion systems, *Adv. Phys.* **36**, 799 (1987).
- [26] G. M. Zhang and L. Yu, Kondo singlet state coexisting with antiferromagnetic long-range order: A possible ground state for Kondo insulators, *Phys. Rev. B* **62**, 76 (2000).
- [27] B. Coqblin, C. Lacroix, M. A. Gusmao, and J. R. Iglesias, Band-filling effects on Kondo-lattice properties, *Phys. Rev. B* **67**, 064417 (2003).
- [28] C. Pépin, M. R. Norman, and A. Ferraz, Modulated Spin Liquid: A New Paradigm for URu₂Si₂, *Phys. Rev. Lett.* **106**, 106601 (2011).
- [29] G. Zhang, J. S. V. Dyke, and R. Flint, Cubic hastatic order in the two-channel Kondo-Heisenberg model, *Phys. Rev. B* **98**, 235143 (2018).
- [30] T. Senthil, S. Sachdev, and M. Vojta, Fractionalized Fermi Liquids, *Phys. Rev. Lett.* **90**, 216403 (2003).
- [31] T. Senthil, M. Vojta, and S. Sachdev, Weak magnetism and non-Fermi liquids near heavy-fermion critical points, *Phys. Rev. B* **69**, 035111 (2004).
- [32] P. Coleman, J. B. Marston, and A. J. Schofield, Transport anomalies in a simplified model for a heavy-electron quantum critical point, *Phys. Rev. B* **72**, 245111 (2005).
- [33] I. Paul, C. Pépin, and M. R. Norman, Kondo Breakdown and Hybridization Fluctuations in the Kondo-Heisenberg Lattice, *Phys. Rev. Lett.* **98**, 026402 (2007).
- [34] I. Paul, C. Pépin, and M. R. Norman, Multiscale fluctuations near a Kondo breakdown quantum critical point, *Phys. Rev. B* **78**, 035109 (2008).
- [35] K. Hanzawa and K. Ohara, Asymptotic local moment formation in the Kondo lattice, *Phys. Rev. B* **76**, 184407 (2007).
- [36] K. Ohara and K. Hanzawa, A Generalized Ginzburg-Landau-Wilson Theory of the Kondo Lattice, *J. Phys. Soc. Jpn.* **82**, 104713 (2013).
- [37] K. Ohara and K. Hanzawa, Nambu-Goldstone and Higgs Modes in the Kondo Insulator, *J. Phys. Soc. Jpn.* **83**, 104604 (2014).
- [38] M. Jiang and Y.-F. Yang, Universal scaling in the Knight-shift anomaly of the doped periodic Anderson model, *Phys. Rev. B* **95**, 235160 (2017).
- [39] M. Jiang, Enhanced tendency towards *d*-wave pairing and antiferromagnetism in a doped staggered periodic Anderson model, *Phys. Rev. B* **102**, 085119 (2020).
- [40] D. Hu, N.-H. Tong, and Y.-F. Yang, Energy-scale cascade and correspondence between Mott and Kondo lattice physics, *Phys. Rev. Research* **2**, 043407 (2020).
- [41] R. Han, D. Hu, J. Wang, and Y.-F. Yang, Schwinger boson approach for the dynamical mean-field theory of the Kondo lattice, *Phys. Rev. B* **104**, 245132 (2021).
- [42] J.-J. Dong, D. Huang, and Y.-F. Yang, Mutual information, quantum phase transition, and phase coherence in Kondo systems, *Phys. Rev. B* **104**, L081115 (2021).
- [43] See Supplemental Material for more details on the theoretical derivation, the numerical algorithm, and the probabilistic distribution of the amplitudes $|F_i|$ and $|B_{ij}|$.
- [44] A. Mukherjee, N. D. Patel, S. Dong, S. Johnston, A. Moreo, and E. Dagotto, Testing the Monte Carlo mean field approximation in the one-band Hubbard model, *Phys. Rev. B* **90**, 205133 (2014).
- [45] S. Pradhan and G. V. Pai, Holstein-Hubbard model at half filling: A static auxiliary field study, *Phys. Rev. B* **92**, 165124 (2015).
- [46] M. Karmakar and P. Majumdar, Population-imbalanced lattice fermions near the BCS-BEC crossover: Thermal physics of the breached pair and Fulde-Ferrell-Larkin-Ovchinnikov phases, *Phys. Rev. A* **93**, 053609 (2016).
- [47] N. D. Patel, A. Mukherjee, N. Kaushal, A. Moreo, and E. Dagotto, Non-Fermi Liquid Behavior and Continuously Tunable Resistivity Exponents in the Anderson-Hubbard Model at Finite Temperature, *Phys. Rev. Lett.* **119**, 086601 (2017).
- [48] H. Ishizuka and Y. Motome, Partial Disorder in an Ising-Spin Kondo Lattice Model on a Triangular Lattice, *Phys. Rev. Lett.* **108**, 257205 (2012).
- [49] W.-W. Yang, J. Zhao, H.-G. Luo, and Y. Zhong, Exactly solvable Kondo lattice model in the anisotropic limit, *Phys. Rev. B* **100**, 045148 (2019).
- [50] M. M. Maska and N. Trivedi, Temperature-driven BCS-BEC crossover and Cooper-paired metallic phase in coupled boson-fermion systems, *Phys. Rev. B* **102**, 144506 (2020).
- [51] S. Saremi, P. A. Lee, and T. Senthil, Unifying Kondo coherence and antiferromagnetic ordering in the honeycomb lattice, *Phys. Rev. B* **83**, 125120 (2011).
- [52] S. Nakatsuji, S. Yeo, L. Balicas, Z. Fisk, P. Schlottmann, P. G. Pagliuso, N. O. Moreno, J. L. Sarrao, and J. D. Thompson, Intersite Coupling Effects in a Kondo Lattice, *Phys. Rev. Lett.* **89**, 106402 (2002).
- [53] Y.-F. Yang, Z. Fisk, H.-O. Lee, J. D. Thompson, and D. Pines, Scaling the Kondo lattice, *Nature* **454**, 611 (2008).
- [54] J. Wang and Y.-F. Yang, Nonlocal Kondo effect and quantum critical phase in heavy-fermion metals, *Phys. Rev. B* **104**, 165120 (2021).
- [55] J. Wang and Y.-F. Yang, Spin current Kondo effect in frustrated Kondo systems, *Sci. China Phys. Mech. Astron.* **65**, 227212 (2022).
- [56] I. Affleck and J. B. Marston, Large-*N* limit of the Heisenberg-Hubbard model: Implications for high-*T_c* superconductors, *Phys. Rev. B* **37**, 3774 (1988).
- [57] T. C. Hsu, Spin waves in the flux-phase description of the *S* = 1/2 Heisenberg antiferromagnet, *Phys. Rev. B* **41**, 11379 (1990).
- [58] X.-G. Wen, Quantum orders and symmetric spin liquids, *Phys. Rev. B* **65**, 165113 (2002).
- [59] T. Hazra and P. Coleman, Luttinger sum rules and spin fractionalization in the SU(*N*) Kondo lattice, *Phys. Rev. Research* **3**, 033284 (2021).
- [60] E. H. Lieb, Flux Phase of the Half-Filled Band, *Phys. Rev. Lett.* **73**, 2158 (1994).
- [61] S. Kumar and P. Majumdar, A travelling cluster approximation for lattice fermions strongly coupled to classical degrees of freedom, *Eur. Phys. J. B* **50**, 571 (2006).
- [62] S. Nakatsuji, D. Pines, and Z. Fisk, Two Fluid Description of the Kondo Lattice, *Phys. Rev. Lett.* **92**, 016401

- (2004).
- [63] N. J. Curro, B. L. Young, J. Schmalian, and D. Pines, Scaling in the emergent behavior of heavy-electron materials, *Phys. Rev. B* **70**, 235117 (2004).
- [64] Y.-F. Yang and D. Pines, Universal Behavior in Heavy-Electron Materials, *Phys. Rev. Lett.* **100**, 096404 (2008).
- [65] C. Gros, Control of the finite-size corrections in exact diagonalization studies, *Phys. Rev. B* **53**, 6865 (1996).
- [66] J. Li, C. Cheng, T. Paiva, H.-Q. Lin, and R. Mondaini, Giant Magnetoresistance in Hubbard Chains, *Phys. Rev. Lett.* **121**, 020403 (2018).

Development of long-range phase coherence on the Kondo lattice

- Supplemental Material -

Jian-Jun Dong^{1,2,3} and Yi-feng Yang^{2,3,4}

¹*Department of Physics and Chongqing Key Laboratory for Strongly Coupled Physics, Chongqing University, Chongqing 401331, China*

²*Beijing National Laboratory for Condensed Matter Physics and Institute of Physics, Chinese Academy of Sciences, Beijing 100190, China*

³*University of Chinese Academy of Sciences, Beijing 100049, China*

⁴*Songshan Lake Materials Laboratory, Dongguan, Guangdong 523808, China*

I. The effective action

To derive the effective action of the Kondo-Heisenberg model, we first use the Abrikosov pseudofermion representation $\mathbf{S}_i = \sum_{\eta\gamma} f_{i\eta}^\dagger \frac{\sigma_{\eta\gamma}}{2} f_{i\gamma}$ to rewrite the Kondo and Heisenberg terms as follows:

$$\begin{aligned} H_K &= J_K \sum_i \mathbf{s}_i \cdot \mathbf{S}_i \\ &= \frac{J_K}{4} \sum_i c_{i\alpha}^\dagger c_{i\alpha} - \frac{J_K}{2} \sum_i c_{i\alpha}^\dagger c_{i\beta} f_{i\alpha} f_{i\beta}^\dagger, \\ H_H &= J_H \sum_{\langle ij \rangle} \mathbf{S}_i \cdot \mathbf{S}_j \\ &= \frac{N_0 J_H}{2} - \frac{J_H}{2} \sum_{\langle ij \rangle} f_{i\alpha}^\dagger f_{i\beta} f_{j\alpha} f_{j\beta}^\dagger, \end{aligned} \quad (S1)$$

where N_0 is the number of lattice sites. The first term of H_K can be absorbed into the definition of the electron chemical potential and the constant term of H_H can be dropped for simplicity. Upon Hubbard-Stratonovich transformations, the above interaction terms can be decomposed as

$$\begin{aligned} H_K &\rightarrow \frac{J_K}{2} \sum_i |V_i|^2 + \frac{J_K}{2} \sum_{i\sigma} \left(V_i c_{i\sigma}^\dagger f_{i\sigma} + \text{H.c.} \right), \\ H_H &\rightarrow \frac{J_H}{2} \sum_{\langle ij \rangle} |\chi_{ij}|^2 + \frac{J_H}{2} \sum_{\langle ij \rangle \sigma} \left(\chi_{ij} f_{i\sigma}^\dagger f_{j\sigma} + \text{H.c.} \right). \end{aligned} \quad (S2)$$

We then obtain a Lagrangian $\mathcal{L} = \mathcal{L}_c + \mathcal{L}_f + \mathcal{L}_K + \mathcal{L}_H$ with

$$\begin{aligned} \mathcal{L}_c &= \sum_{i\sigma} c_{i\sigma}^\dagger (\partial_\tau + \mu) c_{i\sigma} - t \sum_{\langle ij \rangle \sigma} \left[c_{i\sigma}^\dagger c_{j\sigma} + \text{H.c.} \right], \\ \mathcal{L}_f &= \sum_{i\sigma} f_{i\sigma}^\dagger (\partial_\tau + \lambda_i) f_{i\sigma} - \sum_i \lambda_i, \\ \mathcal{L}_K &= \frac{J_K}{2} \sum_i |V_i|^2 + \frac{J_K}{2} \sum_{i\sigma} \left[V_i c_{i\sigma}^\dagger f_{i\sigma} + \text{H.c.} \right], \\ \mathcal{L}_H &= \frac{J_H}{2} \sum_{\langle ij \rangle} |\chi_{ij}|^2 + \frac{J_H}{2} \sum_{\langle ij \rangle \sigma} \left[\chi_{ij} f_{i\sigma}^\dagger f_{j\sigma} + \text{H.c.} \right]. \end{aligned} \quad (S3)$$

Here, c_i and f_i are Grassmann variables, V_i and χ_{ij} are complex variables, and λ_i is the Lagrange multiplier for the constraint $\sum_\sigma f_{i\sigma}^\dagger f_{i\sigma} = 1$.

The partition function is

$$Z = \int \mathcal{D}[c_i, f_i, \lambda_i, V_i, \chi_{ij}] \exp \left[- \int_0^\beta d\tau \mathcal{L}(\tau) \right], \quad (S4)$$

which faithfully represents the original Kondo-Heisenberg model if the functional integrals are performed exactly. We have then the action $S = \int_0^\beta d\tau \mathcal{L}(\tau)$ in the frequency space,

$$\begin{aligned} S &= \sum_{i,l} \frac{\beta J_K |V_{i,l}|^2}{2} + \sum_{\langle ij \rangle, l} \frac{\beta J_H |\chi_{ij,l}|^2}{2} - \sum_i \beta \lambda_i \\ &\quad + \sum_{nm\sigma} \Psi_{n\sigma}^\dagger (O_{nm} - i\omega_n \delta_{nm}) \Psi_{m\sigma}, \end{aligned} \quad (S5)$$

where $\Psi_{n\sigma} = [c_{1\sigma n}, \dots, c_{N_0\sigma n}, f_{1\sigma n}, \dots, f_{N_0\sigma n}]^T$, O_{nm} is the corresponding matrix, and the subscripts l (n/m) denote bosonic (fermionic) Matsubara frequency.

The static approximation assumes time-independent auxiliary field variables: $V_i(\tau) = V_i$ and $\chi_{ij}(\tau) = \chi_{ij}$. In frequency space, this implies $V_{i,n-m} = V_i \delta_{nm}$ and $\chi_{ij,n-m} = \chi_{ij} \delta_{nm}$. Hence $O_{nm} = O \delta_{nm}$, with the block form $O = \begin{bmatrix} T^c & M \\ M^\dagger & T^f \end{bmatrix}$, where T^c (T^f) is the $N_0 \times N_0$ hopping matrix of conduction electrons (pseudofermions), and $M_{ij} = \delta_{ij} J_K V_i / 2$ is a diagonal matrix for their onsite hybridization. Using the integral formula,

$$\int \mathcal{D}[\Psi^\dagger, \Psi] \exp(-\Psi^\dagger M \Psi) = \det M, \quad (S6)$$

we can integrate out all fermionic degrees of freedom and obtain the following effective action,

$$\begin{aligned} S_{\text{eff}} &= \sum_i \frac{\beta J_K |V_i|^2}{2} + \sum_{\langle ij \rangle} \frac{\beta J_H |\chi_{ij}|^2}{2} - \sum_i \beta \lambda_i \\ &\quad - 2 \sum_n \ln \det(O - i\omega_n). \end{aligned} \quad (S7)$$

The partition function is now

$$Z = \int \mathcal{D}[V_i, \chi_{ij}, \lambda_i] \exp(-S_{\text{eff}}), \quad (S8)$$

which is an $8N_0$ -dimensional integral of the auxiliary fields defined on the lattice.

II. The uniform mean-field theory

The uniform mean-field theory assumes a real solution,

$$V_i = \bar{V}_i = V, \quad \chi_{ij} = \bar{\chi}_{ij} = \chi, \quad \lambda_i = \lambda \quad (\text{S9})$$

which turns the high-dimensional integral into a three-dimensional one, $Z = \int \mathcal{D}[V, \chi, \lambda] e^{-S_{\text{eff}}}$. Their mean-field values can be derived from the saddle-point approximation by minimizing the free energy, $F = S_{\text{eff}}/\beta$. From $\partial F/\partial \chi = 0$, $\partial F/\partial V = 0$, and $\partial F/\partial \lambda = 0$, we obtain the self-consistent equations:

$$\begin{aligned} \chi &= -\frac{1}{N_0} \sum_{\mathbf{k}, \eta=\pm} (\cos k_x + \cos k_y) \frac{\eta f(E_{\mathbf{k}, \eta}) (E_{\mathbf{k}, \eta} - \xi_{c\mathbf{k}})}{E_{\mathbf{k}, +} - E_{\mathbf{k}, -}}, \\ V &= -\frac{J_K V}{N_0} \sum_{\mathbf{k}} \left[\frac{f(E_{\mathbf{k}, +}) - f(E_{\mathbf{k}, -})}{E_{\mathbf{k}, +} - E_{\mathbf{k}, -}} \right], \\ 1 &= \frac{2}{N_0} \sum_{\mathbf{k}, \eta=\pm} \frac{\eta f(E_{\mathbf{k}, \eta}) (E_{\mathbf{k}, \eta} - \xi_{c\mathbf{k}})}{E_{\mathbf{k}, +} - E_{\mathbf{k}, -}}, \end{aligned} \quad (\text{S10})$$

where $f(x) = 1/(1 + e^{\beta x})$ is the Fermi distribution function and

$$\begin{aligned} E_{\mathbf{k}, \pm} &= \frac{(\xi_{c\mathbf{k}} + \xi_{f\mathbf{k}}) \pm \sqrt{(\xi_{c\mathbf{k}} - \xi_{f\mathbf{k}})^2 + J_K^2 V^2}}{2}, \\ \xi_{c\mathbf{k}} &= -2t (\cos k_x + \cos k_y), \\ \xi_{f\mathbf{k}} &= \chi J_H (\cos k_x + \cos k_y) + \lambda. \end{aligned} \quad (\text{S11})$$

The particle-hole symmetry requires $\lambda = 0$.

III. The Monte Carlo algorithm

We use the usual Metropolis algorithm for the Monte Carlo sampling of the probability distribution function,

$$p(V_i, \chi_{ij}) = \frac{1}{Z} \exp(-S_{\text{eff}}), \quad (\text{S12})$$

where Z serves as the normalization factor and λ_i have been approximated by their mean-field value $\lambda_i = 0$ for simplicity. The Monte Carlo procedures involve:

- (1) Starting with a random set of configurations

$$\Phi \equiv (V_1^x, V_1^y, \dots, V_{N_0}^x, V_{N_0}^y, \chi_1^x, \chi_1^y, \dots, \chi_{2N_0}^x, \chi_{2N_0}^y), \quad (\text{S13})$$

where we have given a new label (subscript) for the auxiliary variables in the numerical algorithm.

- (2) For each Monte Carlo sweep, we update sequentially one of the $6N_0$ variables in Φ , so that $\Phi'_l = \Phi_l + \Delta \times x$ where x is a random number between -1 and 1 and $\Delta > 0$ is the step length to adjust the accepted probability. Then we calculate the change of the effective action

$$\Delta S = S_{\text{eff}}[\Phi'] - S_{\text{eff}}[\Phi]. \quad (\text{S14})$$

Following the Metropolis algorithm, the proposed configuration Φ'_l is accepted with the probability $\min[1, e^{-\Delta S}]$. This procedure is repeated sequentially for all $6N_0$ variables in Φ .

- (3) Repeating step (2) to thermalize the system.

(4) After thermalization, 200000 Monte Carlo sweep are performed for the Monte Carlo sampling.

(5) Taking one sample (configuration) every 10 sweeps to reduce self-correlations in the data and calculating the physical quantities by average over a total number of 20000 configurations. An illustration of all samples for the local V_i can be found in Fig. 1(d), from which the marginal distribution of $p(V_i)$ can be obtained.

IV. The probabilistic distribution of the amplitudes $|F_i|$ and $|B_{ij}|$

For completeness, we plot in Fig. S1 the probabilistic distribution of the magnitude $p(|B|) \equiv p(|B_{ij}|)$ and $p(|F|) \equiv p(|F_i|)$ with varying Kondo coupling J_K or temperature T . We see a peak in $p(|B|)$ near $|B| = 0$ at small J_K or high T , which shifts to finite $|B|$ for large J_K at low T , reflecting that of $p(|V|)$. The distribution $p(|F|)$ always shows a peak near zero at low T and becomes suppressed at high T , reflecting the increase of the magnetic correlation ($|\chi|$ field) with lowering temperature. These results are consistent with the overall picture derived in the main text.

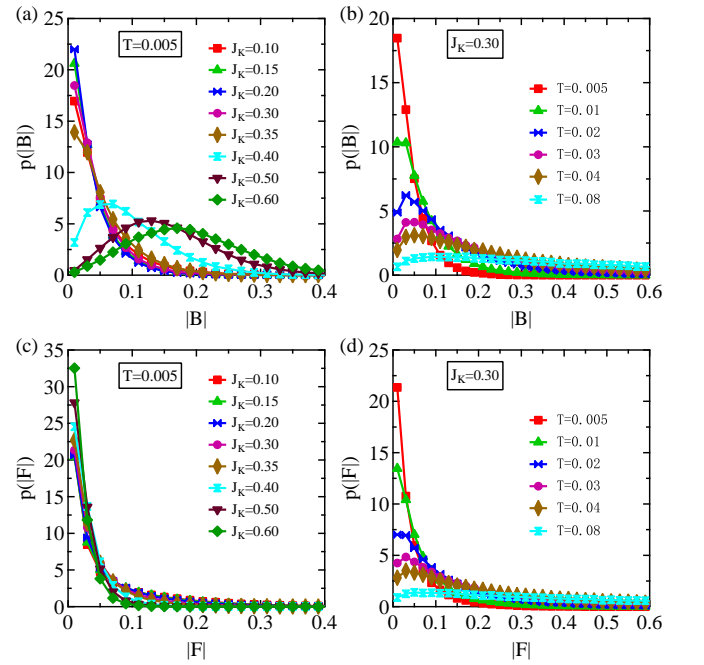


FIG. S1: Probabilistic distribution of (a)(b) $p(|B|)$ and (c)(d) $p(|F|)$ with varying Kondo coupling J_K or temperature T .